Trigger-happy resident memory CD4$^+$ T cells inhabit the human lungs

AE Oja[1], B Piet[1,2], C Helbig[1], R Stark[1], D van der Zwan[1], H Blaauwgeers[3], EB M Remmerswaal[4,5], D Amsen[1], RE Jonkers[6], PD Moerland[7], MA Nolte[1], RAW van Lier[1] and P Hombrink[1]

Resident memory T cells (T$_{RM}$) reside in the lung epithelium and mediate protective immunity against respiratory pathogens. Although lung CD8$^+$ T$_{RM}$ have been extensively characterized, the properties of CD4$^+$ T$_{RM}$ remain unclear. Here we determined the transcriptional signature of CD4$^+$ T$_{RM}$, identified by the expression of CD103, retrieved from human lung resection material. Various tissue homing molecules were specifically upregulated on CD4$^+$ T$_{RM}$, whereas expression of tissue egress and lymph node homing molecules were low. CD103$^+$ T$_{RM}$ expressed low levels of T-bet, only a small portion expressed Eomesodermin (Eomes), and although the mRNA levels for Hobit were increased, protein expression was absent. On the other hand, the CD103$^+$ T$_{RM}$ showed a Notch signature. CD4$^+$CD103$^+$ T$_{RM}$ constitutively expressed high transcript levels of numerous cytotoxic mediators that was functionally reflected by a fast recall response, magnitude of cytokine production, and a high degree of polyfunctionality. Interestingly, the superior cytokine production appears to be because of an accessible interferon-γ (IFNγ) locus and was partially because of rapid translation of preformed mRNA. Our studies provide a molecular understanding of the maintenance and potential function of CD4$^+$ T$_{RM}$ in the human lung. Understanding the specific properties of CD4$^+$ T$_{RM}$ is required to rationally improve vaccine design.

INTRODUCTION

The lung is one of the most fascinating and intricate immunological sites of the human body. The lower respiratory tract is covered with a 75 m^2 monolayer of epithelial cells that separate the outside world from the underlying vasculature and protect the interstitial tissue. Although the lungs are constantly exposed to pollutants and airborne microbes, pathogens seldom manage to cause disease, as most are met with appropriate local immune responses. Once elicited, respiratory infections and ensuing immune responses can have severe consequences for the vital gas exchange. Therefore, the balance between immune protection and prevention of immunopathology must be carefully regulated.

Annually, respiratory viruses are a major cause of morbidity and mortality worldwide, especially among the young, elderly, and immunocompromised individuals. Despite reports demonstrating a role of lung CD4$^+$ T cells in protecting against airborne infections,[1–3] their characteristics and mode of action remain to be determined. Significant numbers of CD4$^+$ T cells, even outnumbering CD8$^+$ T cells, were demonstrated to be present in the lungs of healthy individuals.[4] It is unclear whether lung CD4$^+$ T cells predominantly mediate helper functions by engaging local B cells and supporting CD8$^+$ T cells or whether they locally execute immune effector functions. In fact, lung CD4$^+$ T cells could be functionally multifaceted as they were shown, in mouse infection models, to drive recruitment of other immune effectors to the inflamed site[1] and promote development of protective resident CD8$^+$ CD103$^+$ T cells in the lung epithelium.[5] To what extent similar mechanisms operate in human lungs remains unclear.

Upon pathogen encounter naive T (T$_N$) cells can differentiate into several types of memory T cells. These memory subtypes

[1]Department of Hematopoiesis, Sanquin Research and Landsteiner Laboratory, Amsterdam, The Netherlands. [2]Department of Respiratory Medicine, OLVG, Amsterdam, The Netherlands. [3]Department of Pathology, OLVG, Amsterdam, The Netherlands. [4]Department of Experimental Immunology, Academic Medical Center, Amsterdam, The Netherlands. [5]Renal Transplant Unit, Division of Internal Medicine, Academic Medical Center, Amsterdam The Netherlands. [6]Department of Respiratory Medicine, Academic Medical Center, Amsterdam, The Netherlands and [7]Department of Clinical Epidemiology, Biostatistics and Bioinformatics and Department of Immunology, Academic Medical Center, Amsterdam, The Netherlands. Correspondence: AE Oja or P Hombrink (a.oja@sanquin.nl or p.hombrink@sanquin.nl)

can be phenotypically separated into central memory (T_{CM}), effector memory (T_{EM}), and resident memory (T_{RM}) T cells.[6–9] Whereas T_{EM} and T_{CM} migrate almost exclusively through blood and lymphoid tissue, T_{RM} are restricted to nonlymphoid tissues, such as the lungs,[1,5,10–13] brain,[14,15] skin,[16,17] and vaginal mucosa.[18,19] T_{RM} can be defined by the expression of CD69, an inhibitor of S1PR1 function, that prevents cells from exiting the tissue.[20] Further, downregulation of S1PR1 is necessary for the establishment of CD8$^+$ T_{RM}.[21] Epithelial T_{RM} can in addition be defined by the expression of CD103, the α_E subunit of the $\alpha_E\beta_7$ integrin that is required to dock these cells to the E-cadherin-expressing epithelial cells.[22,23] This interaction may be crucial for T_{RM} barrier function, as it retains the T_{RM} at the entry site of pathogens, thus allowing for their fast recognition. This notion is corroborated by the enrichment of respiratory virus-specific CD8$^+$ T cells in the CD103$^+$ fraction of the human lung.[11] Although murine CD4$^+$ T_{RM} express similar surface molecules as CD8$^+$ T_{RM},[2,10] their precise characteristics and molecular imprints are not as well defined. Nevertheless there are several indications pointing toward the important role of CD4$^+$ T_{RM} in protection against respiratory infections. CD4$^+$ T cells are necessary for the formation of protective CD8$^+$ T_{RM} during primary influenza infection.[5] This function would be in line with traditional helper cell function described for CD4$^+$ T cells.[24–29] In addition, lung CD4$^+$ T_{RM} themselves protect against lethal influenza challenge, whereas spleen CD4$^+$ T cells do not.[2] The precise mechanism(s) for direct effector functions executed by CD4$^+$ lung T_{RM} are ill defined, although several reports point toward a helper-independent function operated by interferon-γ (IFNγ)[1,3] and cytotoxic molecules.[30,31]

Here we analyzed the genetic program of CD4$^+$CD103$^+$ T cells obtained from human lungs. By determining the minimal core transcriptional signature, we demonstrated that lung CD4$^+$ CD103$^+$ T cells represent a unique subset of CD4$^+$ T cells that are very different from blood CD4$^+$ T cells but closely related to lung CD8$^+$CD103$^+$ T_{RM}.[13] In contrast to what was previously demonstrated for CD4$^+$ memory T cells in the skin,[30,31] our data suggest that CD4$^+$CD103$^+$ T cells from the lung represent a genuine resident population that is unlikely to equilibrate with the circulation. We identified a set of chemokine receptors and adhesion molecules that allow CD4$^+$ T_{RM} to migrate and persist in the lungs. Furthermore, lung CD4$^+$CD103$^+$ T_{RM} constitutively expressed mRNA encoding various effector molecules and produced multiple cytokines upon stimulation. The magnitude of this response was not only more robust than that of circulating CD4$^+$ T-cell subsets, but also faster and highly polyfunctional. Our findings suggest that targeting the generation of CD4$^+$ T_{RM} in the lung would be an attractive approach for future vaccine strategies and immunotherapies.

RESULTS

Lung CD4$^+$ T_{RM} are phenotypically distinct from circulating CD4$^+$ T cells

We found that CD4$^+$ T cells were abundantly present in human lungs of patients undergoing partial lung resection, and at similar frequencies as in paired blood (**Figure 1a**). To identify CD4$^+$ T_{RM} in human lung tissue, we analyzed the surface expression of CD103 and CD69 on CD4$^+$ T cells in these samples. Lung, but not paired blood, CD4$^+$ T cells could be divided into three populations based on the expression of CD69 and CD103 (**Figure 1b** and **Supplementary Figure S1** online). The most abundant population in the lung was CD103$^-$ CD69$^+$ that represented 50% of total CD4$^+$ T cells (**Figure 1c**). The expression of CD103 varied among the patients, as 10 to 60% (average 20%) of lung CD4$^+$ T cells were CD103$^+$CD69$^+$. In parallel, we determined the differentiation stage of lung CD4$^+$ T cells by evaluating the surface expression of CD27 and CD45RA (**Figure 1d,e**). Both CD103$^+$CD69$^+$ (95%) and CD103$^-$CD69$^+$ (60%) subsets were enriched for cells with a CD45RA$^-$CD27$^-$ (in blood referred to as T_{EM}) phenotype (**Figure 1e**). Furthermore, virtually all of the lung CD4$^+$ T cells (both CD69$^+$ and CD69$^-$ cells) lacked expression of lymph node-homing chemokine receptor CCR7 (**Figure 1f**, left and middle) that was abundant and restricted to CD45RA$^+$CD27$^+$ naive (T_N) and CD45RA$^-$CD27$^+$ memory (T_M) cells in blood (**Figure 1f**, right). Expression of the costimulatory molecule CD28 was confined to a large proportion of lung CD103$^-$CD69$^+$ T cells and, with the exception of CD45RA$^+$CD27$^-$ effector T cells, to all other blood subsets (**Figure 1g**).

On average, 20% of the lung CD4$^+$ T cells expressed neither CD69 nor CD103 (**Figure 1c**). Although we currently do not have ways to distinguish the potential T_{RM} from the circulating T cells in humans, it should be noted that based on the low expression of CD28 it is unlikely that the majority of these cells belong to the circulating pool. For the remainder of the study we focused on the analysis of the epithelium-dwelling CD103$^+$CD69$^+$ fractions and use CD103$^-$CD69$^+$ T cells and blood-derived CD4$^+$ T-cell subsets as a comparison. We will refer to lung CD4$^+$CD103$^+$CD69$^+$ T cells as CD103$^+$ T_{RM}.

Lung CD103$^+$ T_{RM} have a distinct transcriptional profile compared with circulating CD4$^+$ T cells

To determine the gene expression profile of lung CD4$^+$ T_{RM}, we isolated mRNA from CD4$^+$CD103$^+$ T cells directly after isolation and performed microarray analysis. The lung CD4$^+$CD103$^+$ T_{RM} gene expression profile was compared with peripheral blood CD4$^+$ T-cell subsets to decipher a T_{RM} core signature. CD103$^+$ T_{RM} were sorted from non-cancerous lobectomy tissues of five patients with non-small-cell lung carcinoma and simultaneously peripheral blood-derived memory and naive CD4$^+$ T-cell populations were sorted from five healthy donors. The core lung CD103$^+$ T_{RM} signature was identified by comparing the transcriptome of CD103$^+$ T_{RM} with that of blood T_{EM} (CD45RA$^-$CD27$^-$), T_M (CD45RA$^-$CD27$^+$), and T_N (CD45RA$^+$CD27$^+$) populations (**Figure 2a**). CD4$^+$CD103$^+$ T_{RM} differentially expressed 512 genes (**Supplementary Table S1**). In accordance with their predominant CD45RA$^-$CD27$^-$ phenotype, the CD103$^+$ T_{RM} transcriptional profile proved most similar to the profile of
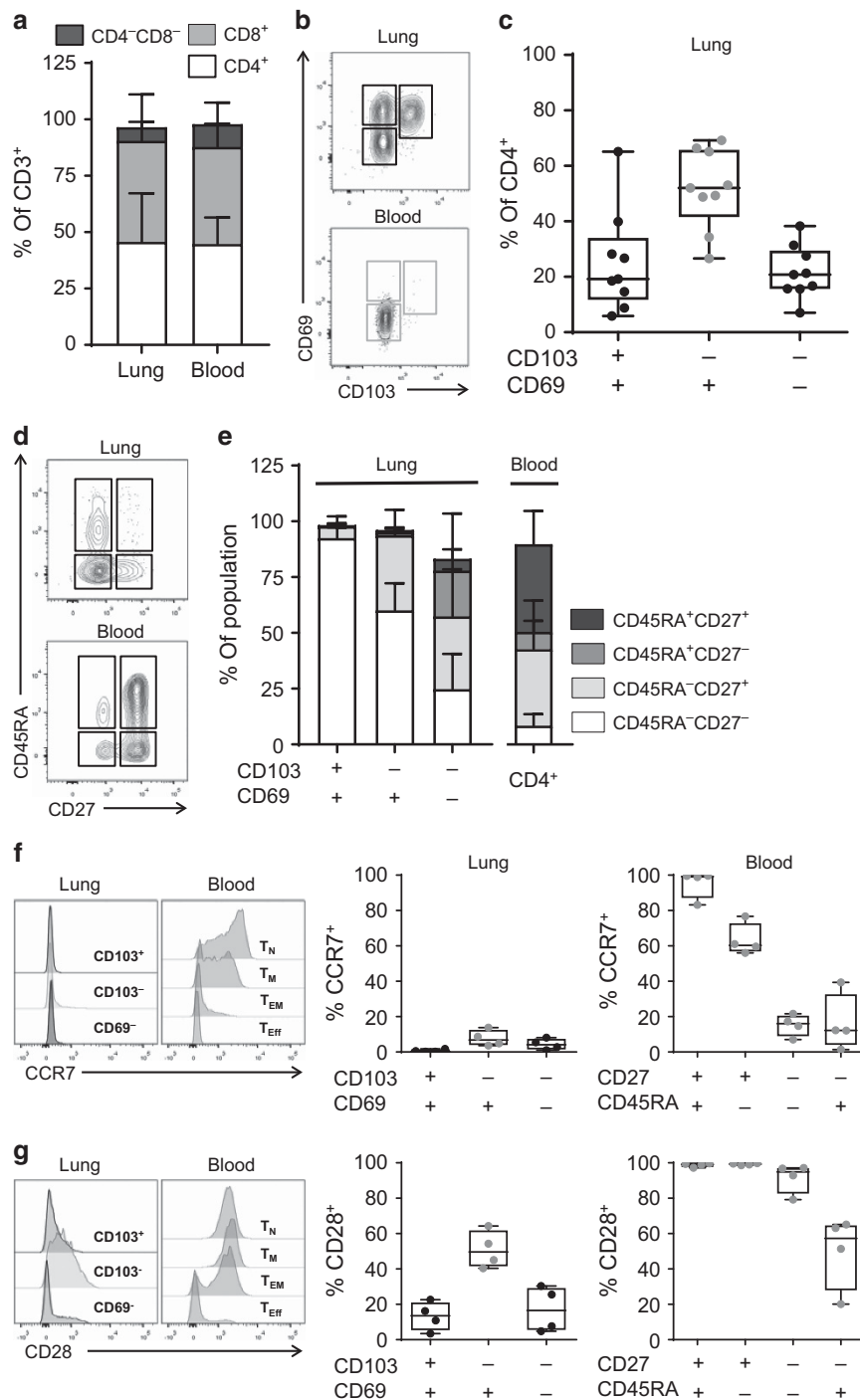
Figure 1 Lung CD4$^+$ T$_{RM}$ have a distinct phenotype compared with circulating CD4$^+$ T cells. (**a**) Quantification of the number of CD4$^-$CD8$^-$ (dark gray), CD8$^+$ (light gray), and CD4$^+$ (white) as percentage of CD3$^+$ T cells was analyzed by flow cytometry for paired lung and blood samples (**b,c**) The expression of CD69 and CD103 on CD4$^+$ T cells derived from paired lung and blood samples, shown by representative contour plots (**b**) and quantification as percentage of CD4$^+$ T cells (**c**). (**d**) The expression of CD27 and CD45RA was determined on lung CD4$^+$CD103$^+$CD69$^+$, CD4$^+$CD103$^-$CD69$^+$, and CD4$^+$CD69$^-$CD103$^-$ and total blood CD4$^+$ T-cell subsets, shown by representative contour plots. (**e**) The frequency of CD45$^+$CD27$^+$ (dark gray), CD45RA$^+$CD27$^-$ (medium gray), CD45RA$^-$CD27$^+$ (light gray), and CD45RA$^-$CD27$^-$ (white) T-cell subsets was determined in lung CD4$^+$CD103$^+$CD69$^+$, CD4$^+$CD103$^-$CD69$^+$, and CD4$^+$CD103$^-$CD69$^-$, and total blood CD4$^+$ T cells. (**f,g**) The expression of CCR7 (**f**) and CD28 (**g**) was quantified as percentage on lung CD4$^+$CD103$^+$CD69$^+$, CD4$^+$CD103$^-$CD69$^+$, and CD4$^+$CD103$^-$CD69$^-$, and blood T$_{EM}$ CD4$^+$CD45RA$^-$CD27$^-$, T$_M$ CD4$^+$CD45RA$^-$CD27$^+$, T$_{eff}$ CD4$^+$CD45RA$^+$CD27$^-$, and T$_N$ CD4$^+$CD45RA$^+$CD27$^+$ T-cell subsets. The histogram overlays (maximum set to 100%) show the expression of CCR7 (**f**) and CD28 (**g**) on a representative lung CD4$^+$CD103$^+$CD69$^+$ (gray), CD4$^+$CD103$^-$CD69$^+$ (gray), and CD4$^+$CD103$^-$CD69$^-$ (black) population and blood T$_{EM}$ CD4$^+$CD45RA$^-$CD27$^-$, T$_M$ CD4$^+$CD45RA$^-$CD27$^+$, T$_{eff}$ CD4$^+$CD45RA$^+$CD27$^-$, and T$_N$ CD4$^+$CD45RA$^+$CD27$^+$ T-cell subsets. (**a–e**) $n = 7$–9 and (**f,g**) $n = 4$. (**a,e**) The quantifications are shown as bar graphs with the mean (± s.d.). (**c,f,g**) The quantifications are shown as box–whisker plots with min–max. Each symbol depicts an individual sample; horizontal line shows the median. (**a–e**) Paired lung–blood samples. (**f,g**) Blood from healthy donors. T$_{EM}$, effector memory T cell; T$_M$, memory T cell; T$_N$, naive T cell; T$_{RM}$, resident memory T cell.

peripheral blood T_{EM}, followed by T_M and T_N with 649, 1,178, and 2,438 genes differentially expressed, respectively.

Human lung $CD4^+CD103^+$ T_{RM} expressed high transcript levels of *ITGAE*, *CTLA4*, and *ICOS*. On the other side, the expression of *S1PR1*, and the lymph node-homing molecules, *SELL* and *CCR7*, was low (**Figure 2b**), suggesting that the $CD4^+CD103^+$ T_{RM} are retained in the tissue and unlikely recirculate. A similar trend was observed for KLF2 (**Supplementary Figure S2**) that drives expression of S1PR1. We validated a number of these genes by quantitative PCR (**Supplementary Figure S2**). Among the 100 most differentially expressed genes between $CD103^+$ T_{RM} and peripheral T_{EM} cells were genes encoding for transcription factors mediating effector T-cell differentiation and function (*ERG2*, *EPAS1*, and *BATF*), solute carrier family members mediating amino acid transport (*SLC7A5*, *SLC1A5*), a chemokine receptor (*CXCR6*), a cytokine receptor (*IL21R*), a cytokine (*TGFB1*), and fatty-acid-binding protein (*FABP5*), a molecule critical for free fatty acid uptake and in return survival of skin $CD8^+$ T_{RM}[32] (**Figure 2c**). All of these genes demonstrated high expression levels in the $CD103^+$ T_{RM}. $CD103^+$ T_{RM} expressed low levels of several factors mediating WNT pathway signaling (*TCF7*, *WNT7A*), a guanyl nucleotide exchange factor (*RASGRP2*), and *ICAM2*, an adhesion molecule regulating adhesion between immune cells.

To identify genes that may be specifically expressed by lung $CD4^+CD103^+$, but not $CD8^+CD103^+$ T_{RM}, we compared the above identified T_{RM} core signature with that of our previous report on lung $CD8^+$ T_{RM}.[13] We found an overall strong resemblance between both signatures (**Figure 2d**). Although blood $CD4^+$ and $CD8^+$ T cells are generally accepted to be very distinct from each other, these data indicate that the lung niche induces a similar transcriptional imprint on the two T-cell lineages and suggest that the mechanisms involved to retain $CD4^+$ and $CD8^+$ T cells in the lung tissue are alike. Only very few genes were uniquely upregulated by $CD4^+CD103^+$ T_{RM}. Among these were the lysosomal vesicle marker *LAMP2* and transcriptional corepressor *TLE*. The complete list of genes, in alphabetical order, and the corresponding $\log_2$ fold changes are listed in **Supplementary Table S2**. As among the circulating subsets, the T_{EM} appeared most closely related to the lung T_{RM}, we focus on the comparison of lung T_{RM} and blood T_{EM} in the remainder of the article.
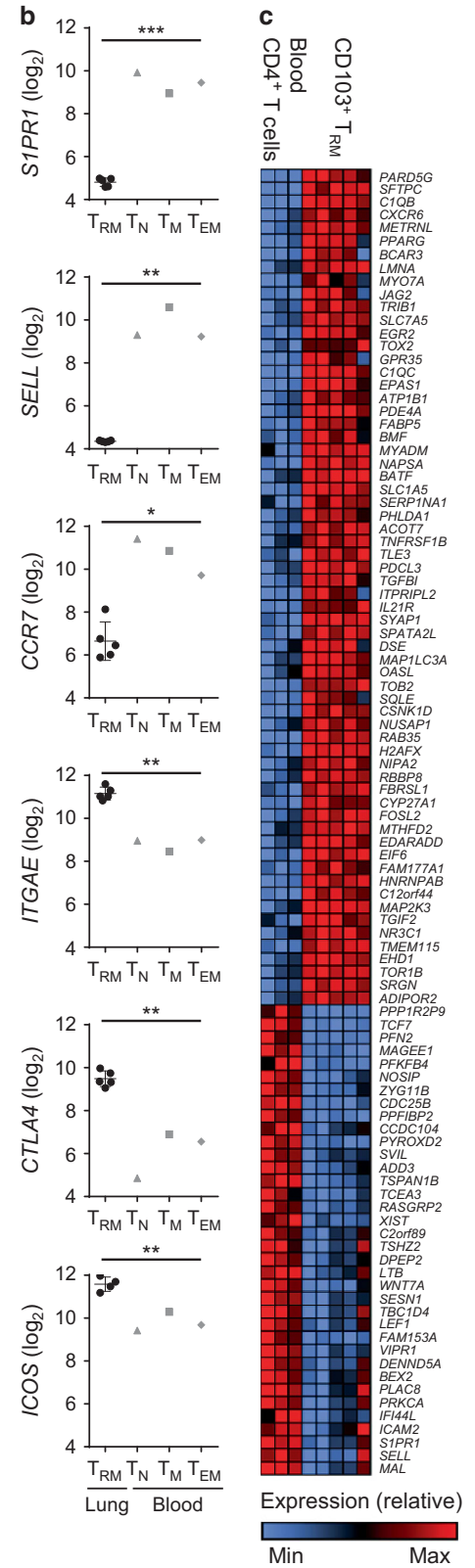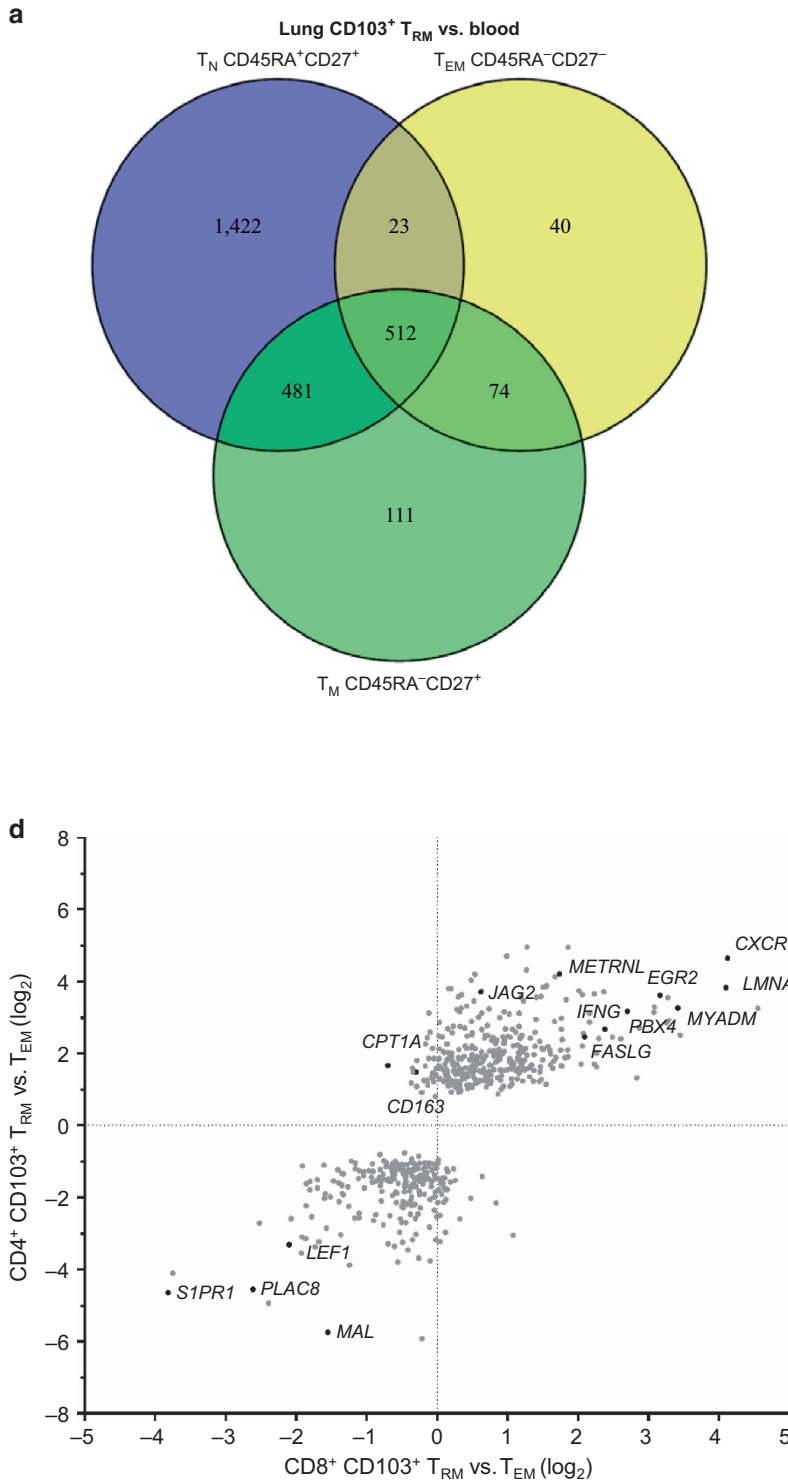
Differential expression of homing molecules by lung $CD4^+$ T_{RM}

$CD4^+$ T_{RM} are anchored in the lung tissue. In mice, their persistence is mediated by specific adhesion molecules that prevent recirculation and allow migration in the tissue.[33,34] Besides the expression of CD103, which helps T_{RM} dock to E-cadherin in epithelia,[22,23] lung $CD4^+CD103^+$ T_{RM} exhibited high mRNA levels of various other integrins and adhesion molecules reflecting this unique property of T_{RM} (**Figure 3a**). Relative to circulating T_{EM}, $CD103^+$ T_{RM} demonstrated low mRNA levels for *ICAM2* (also known as CD102) and high levels of ICAM1 (also known as CD54), a pattern associated with

lymphocyte activation.[35] $CD103^+$ T_{RM} also expressed high levels of the integrin VLA-1 (encoded by *ITGA1*). As T_{RM} that express CD69 but lack CD103 have been described,[36] we also compared the protein expression of homing molecules between the lung-derived $CD103^-CD69^+$ T cells (referred to as $CD103^-$ T_{RM}) and $CD103^+$ T_{RM}. Protein expression of VLA-1 was mainly restricted to $CD103^+$ T_{RM}, as only a part of the $CD103^-$ T_{RM} and very few of the peripheral T_{EM} expressed VLA-1 (**Figure 3b**). Whereas CD97, G-protein-coupled receptor, is expressed by all T cells, increased expression levels of CD97 were found for the $CD103^+$ T_{RM} and are also shared by lung $CD8^+CD103^+$ T_{RM}[13] and intestinal lamina propria $CD8^+$ T_{RM}.[37] Chemokine receptors that distinguished lung $CD103^+$ T_{RM} from peripheral T_{EM} include *CCR7*, *CXCR6*, and *CXCR3* (**Figure 3c**). Whereas downregulation of CCR7 impairs T-cell homing to lymph nodes,[38] expression of CXCR6 and CXCR3 is associated with T-cell recruitment to inflamed tissues.[39,40] Elevated levels of these two chemokine receptors were confirmed at protein level for both $CD103^+$ T_{RM} and $CD103^-$ T_{RM} subsets (**Figure 3d**). We also found both $CD4^+$ T_{RM} subsets to express CCR5 protein (**Figure 3d**), another chemokine receptor associated with lymphocyte recruitment during inflammation.[41] In summary, consistent with their unique location, lung $CD4^+$ T_{RM} expressed specialized profiles of adhesion molecules and chemokine receptors that distinguish them from peripheral $CD4^+$ T cells.

Transcription factor expression by lung $CD4^+$ T_{RM}

T-cell differentiation and function are regulated by networks of transcription factors. For peripheral blood $CD4^+$ T cells, the T-box and RORγt transcription factors are known to drive T helper 1 (Th1) and Th17 cell function, respectively.[24] In mice, the synergistic downregulation of Eomesodermin (Eomes) and T-bet was demonstrated to be a requirement for the formation of $CD8^+$ T_{RM}.[42] In addition, it has recently become appreciated that Blimp1 and Hobit (encoded by *PRDM1* and *ZNF683*, respectively) regulate the programming of $CD8^+$ T_{RM} in mice.[43] To investigate whether similar mechanisms underlie $CD4^+$ T_{RM} formation in the human lungs, we analyzed the expression of these transcription factors. The levels of T-bet and Eomes mRNA transcripts were not elevated in $CD103^+$ T_{RM} when compared with blood T_{EM} cells (**Figure 4a**). In addition, lung $CD103^+$ T_{RM} transcript levels of *PRDM1* and *ZNF683* were slightly upregulated when compared with blood T_{EM}. In line with mRNA levels, protein expression of T-bet and Eomes was intermediate to low in both $CD103^+$ and $CD103^-$ T_{RM} (**Figure 4b**). Furthermore, $CD103^+$ T_{RM} lacked Hobit protein expression whereas a proportion of blood T_{EM} expressed Hobit (**Figure 4b**). This is in accordance with our observation that the $CD4^+CD28^-$ T cells that form a subpopulation within the T_{EM} compartment express high levels of Hobit.[44] We could not address Blimp1 protein expression because of the lack of reliable antibodies. To investigate whether $CD4^+CD103^+$ T_{RM} have a Th2, Th17, or regulatory transcriptional identity, we determined the expression of *GATA-3*, *RORC*, and *FOXP3*. The

a Lung CD103+ T_{RM} vs. blood

T_N CD45RA+CD27+ T_{EM} CD45RA−CD27−

1,422   23   40

481   512   74

111

T_M CD45RA−CD27+

b

$S1PR1$ (log$_2$)   ***

T_{RM} T_N T_M T_{EM}

$SELL$ (log$_2$)   **

T_{RM} T_N T_M T_{EM}

$CCR7$ (log$_2$)   *

T_{RM} T_N T_M T_{EM}

$ITGAE$ (log$_2$)   **

T_{RM} T_N T_M T_{EM}

$CTLA4$ (log$_2$)   **

T_{RM} T_N T_M T_{EM}

$ICOS$ (log$_2$)   **

T_{RM} T_N T_M T_{EM}
Lung   Blood

c

Blood CD4+ T cells / CD103+ T_{RM}

PARD5G, SFTPC, C1QB, CXCR6, METRNL, PPARG, BCAR3, LMNA, MYO7A, JAG2, TRIB1, SLC7A5, EGR2, TOX2, GPR35, C1QC, EPAS1, ATP1B1, PDE4A, FABP5, BMF, MYADM, NAPSA, BATF, SLC1A5, SERP1NA1, PHLDA1, ACOT7, TNFRSF1B, TLE3, PDCL3, TGFBI, ITPRIPL2, IL21R, SYAP1, SPATA2L, DSE, MAP1LC3A, OASL, TOB2, SQLE, CSNK1D, NUSAP1, RAB35, H2AFX, NIPA2, RBBP8, FBRSL1, CYP27A1, FOSL2, MTHFD2, EDARADD, EIF6, FAM177A1, HNRNPAB, C12orf44, MAP2K3, TGIF2, NR3C1, TMEM115, EHD1, TOR1B, SRGN, ADIPOR2, PPP1R2P9, TCF7, PFN2, MAGEE1, PFKFB4, NOSIP, ZYG11B, CDC25B, PPFIBP2, CCDC104, PYROXD2, SVIL, ADD3, TSPAN1B, TCEA3, RASGRP2, XIST, C2orf89, TSHZ2, DPEP2, LTB, WNT7A, SESN1, TBC1D4, LEF1, FAM153A, VIPR1, DENND5A, BEX2, PLAC8, PRKCA, IFI44L, ICAM2, S1PR1, SELL, MAL

Expression (relative)
Min   Max

d

CD4+ CD103+ T_{RM} vs. T_{EM} (log$_2$)

CXCR6, LMNA, METRNL, EGR2, JAG2, MYADM, PBX4, IFNG, FASLG, CPT1A, CD163

LEF1, S1PR1, PLAC8, MAL

CD8+ CD103+ T_{RM} vs. T_{EM} (log$_2$)

CD103$^+$ T$_{RM}$ did not exhibit differential mRNA expression of these transcription factors and very few T cells in the lungs expressed Foxp3 protein (**Supplementary Figure S3a,b**). In search of other transcription factors that may be involved in the regulation of lung CD4$^+$CD103$^+$ T$_{RM}$, we identified a set

of transcription factors among the core signature described above (**Figure 2**). Interestingly, we found CD103$^+$ T$_{RM}$ to express both *BATF* and *IRF4*, transcription factors required for the maintenance of T$_{RM}$ in adipose tissue[45] (**Figure 4c**). Furthermore, the expression of *EGR2* was increased in the
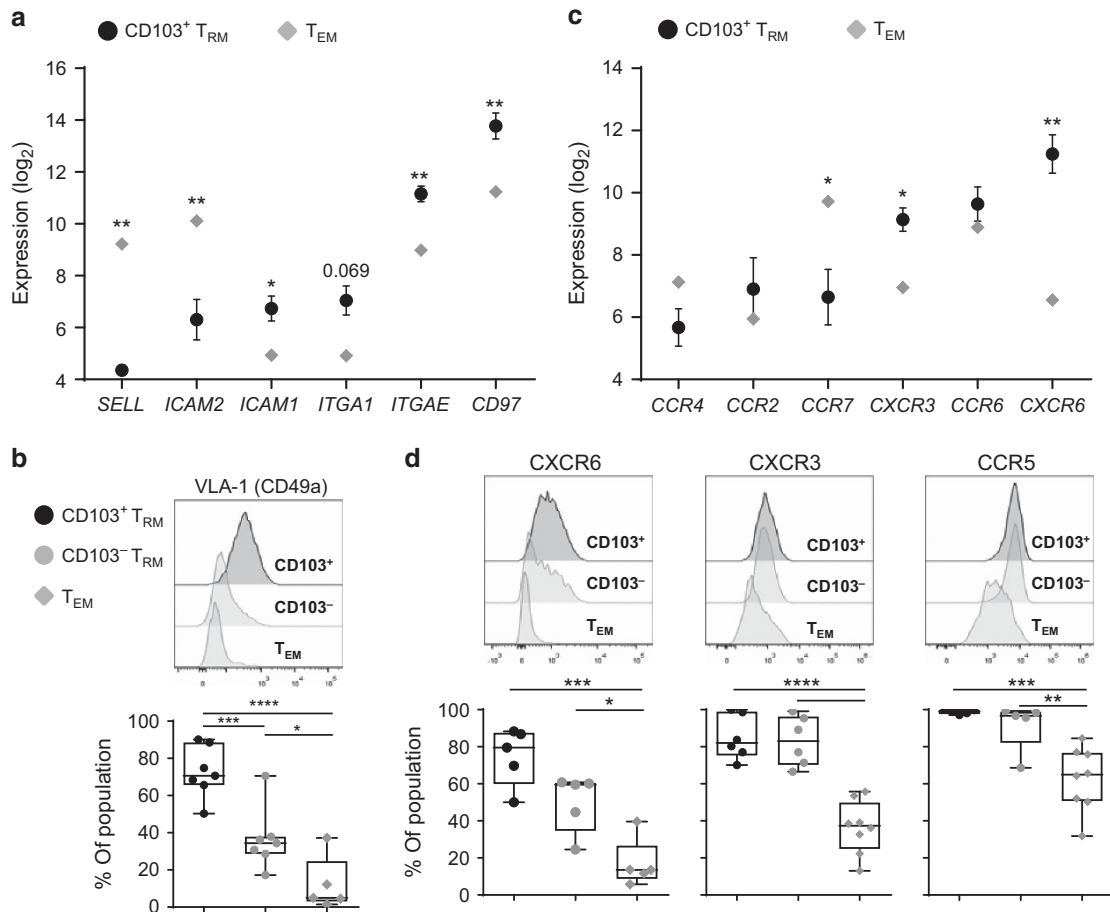
Figure 3 Differential expression of homing molecules by CD4$^+$ T$_{RM}$. (**a,c**) The expression of genes encoding integrins (**a**) and chemokine receptors (**c**) by lung CD103$^+$ T$_{RM}$ (black circle) and blood T$_{EM}$ (gray diamond) was analyzed. (**b,d**) The protein expression of VLA-1 (**b**) and of CXCR6, CXCR3, and CCR5 (**d**) was analyzed on lung CD103$^+$ T$_{RM}$ (black circles), CD103$^-$ T$_{RM}$ (gray circles), and blood T$_{EM}$ (gray diamonds) and is shown by representative histogram overlay (maximum set to 100%) and quantification of percentage of the population. (**a,c**) The *y* axes show log$_2$-transformed normalized values. Each symbol depicts the mean (± s.d.). *False-discovery rate (FDR) < 0.05, **FDR < 0.01; $n = 5$ for lung samples. For the blood samples, five individually sorted samples were pooled before the microarray analysis. (**b,d**) The quantifications are shown as box–whisker plots with min–max. Each symbol depicts an individual sample; horizontal line shows the median; $n = 5$–8. *$P < 0.05$, **$P < 0.01$, ***$P < 0.001$, and ****$P < 0.0001$; 1-way analysis of variance (ANOVA) with Holm–Sidak multiple comparison test. (**a–d**) Blood from healthy donors. T$_{EM}$, effector memory T cell; T$_{RM}$, resident memory T cell.

Figure 2 Lung CD103$^+$ T$_{RM}$ have a unique transcriptional profile compared with circulating CD4$^+$ T cells. A microarray analysis was performed on sorted CD4$^+$CD103$^+$ T cell from lung and CD4$^+$CD45RA$^-$CD27$^-$, CD4$^+$CD45RA$^-$CD27$^+$, and CD4$^+$CD45RA$^+$CD27$^+$ T cells from blood. (**a**) The CD103$^+$ T$_{RM}$ core signature was determined as the genes differentially expressed between lung CD103$^+$ T$_{RM}$ and blood T$_{EM}$ CD45RA$^-$CD27$^-$ (yellow), T$_M$ CD45RA$^-$CD27$^+$ (green), and T$_N$ CD45RA$^+$CD27$^+$ (blue) (based on significance with a false-discovery rate (FDR) of < 0.05). The core signature was defined as the genes differentially expressed between the T$_{RM}$ and all three blood populations, shown in the middle of the Venn diagram. (**b**) The expression of selected genes (*S1PR1, SELL, CCR7, ITGAE, CTLA4, ICOS*) was compared between CD103$^+$ T$_{RM}$ (black circle) and blood T$_N$ CD45RA$^+$CD27$^+$ (gray triangle), T$_M$ CD45RA$^-$CD27$^+$ (gray square), and T$_{EM}$ CD45RA$^-$CD27$^-$ (gray diamond). (**c**) Top 100 significantly different genes are depicted from the CD103$^+$ T$_{RM}$ core signature (from Venn diagram). (**d**) The lung CD4$^+$CD103$^+$ T$_{RM}$ core signature was compared with lung CD8$^+$CD103$^+$ T$_{RM}$. The dot plot shows the genes that are up- and downregulated by CD4$^+$CD103$^+$ T$_{RM}$ compared with blood CD4$^+$ T$_{EM}$ on the *y* axis and up- and downregulated genes by CD8$^+$CD103$^+$ T$_{RM}$ compared with blood CD8$^+$ T$_{EM}$ on the *x* axis. (**b,d**) The *y* axes show log$_2$-transformed normalized values. (**b**) Each symbol depicts the mean (± s.d.). *FDR < 0.05, **FDR < 0.01, and ***FDR < 0.001; $n = 5$ for lung samples. For the blood samples, five individually sorted samples were pooled before the microarray analysis. (**a–d**) Blood from healthy donors. T$_{EM}$, effector memory T cell; T$_M$, memory T cell; T$_N$, naive T cell; T$_{RM}$, resident memory T cell.
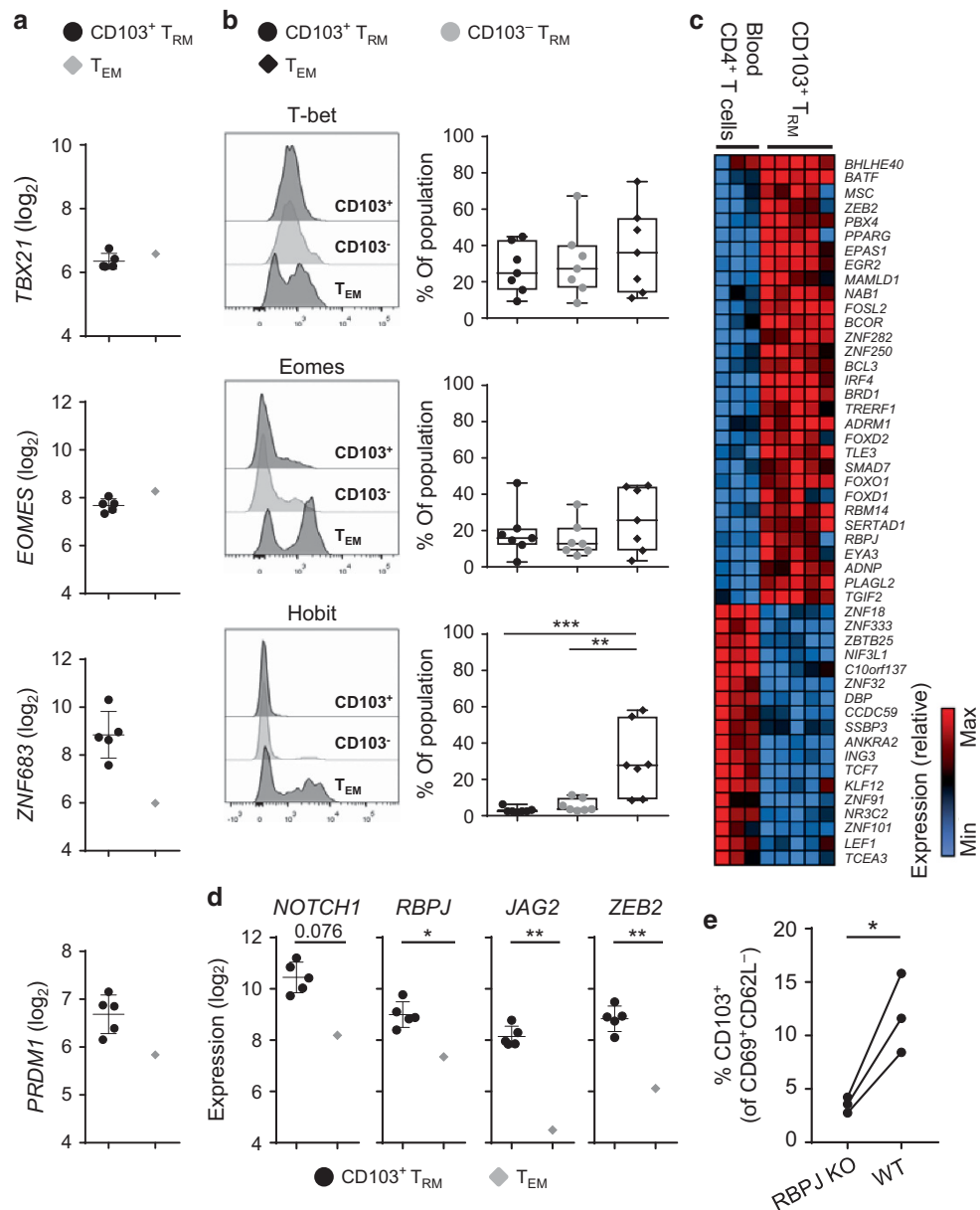
Figure 4 Transcription factor expression by lung CD4$^+$ T$_{RM}$. (**a**) The expression of genes encoding T-bet (*TBX21*) Eomes (*EOMES*), Hobit (*ZNF683*), and Blimp-1 (*PRDM1*) by lung CD103$^+$ T$_{RM}$ (black circles), and blood T$_{EM}$ (gray diamonds) was determined. (**b**) The protein expression of T-bet, Eomes, and Hobit was determined for lung CD103$^+$ T$_{RM}$ (black circles), CD103$^-$ T$_{RM}$ (gray circles), and blood T$_{EM}$ (black diamonds) and is shown by representative histogram overlay (maximum set to 100%) and quantification of percentage of the population. (**c**) The expression of genes encoding transcription factors in the CD103$^+$ T$_{RM}$ core signature is depicted for lung CD103$^+$ T$_{RM}$ and blood T$_N$, T$_M$, and T$_{EM}$ (shown as Blood CD4$^+$ T cells). (**d**) The expression of Notch-related genes (*NOTCH1*, *RBPJ*, *JAG2*, and *ZEB2*) was quantified for lung CD103$^+$ T$_{RM}$ (black circles), and blood T$_{EM}$ (gray diamonds). (**e**) The frequency of CD103$^+$ T$_{RM}$ of CD69$^+$CD62L$^-$CD1d$^-$ Foxp3$^-$ CD4$^+$ T cells in lungs of steady-state *RBPJ$^{fl/fl}$Cd4-Cre$^+$* (RBPJ KO) and *RBPJ$^{fl/fl}$Cd4-Cre$^+$* (wild-type (WT)) littermate mice. (**a**,**d**) The *y* axes show log$_2$-transformed normalized values. Each symbol depicts an individual sample; horizontal line shows the mean (± s.d.). *False-discovery rate (FDR) < 0.05, **FDR < 0.01; $n = 5$ for lung samples. For the blood samples, five individually sorted samples were pooled before the microarray analysis. (**b**) The quantifications are shown as box–whisker plots with min–max. Each symbol depicts an individual sample; horizontal line shows the median; $n = 7$; paired samples. **$P < 0.01$ and ***$P < 0.001$; 1-way analysis of variance (ANOVA) with Holm–Sidak multiple comparison test. (**e**) Each symbol depicts an individual mouse; $n = 3$; paired littermates. *$P < 0.05$ (paired *T*-test). Data represent three experiments. (**a**–**d**) For the blood subsets, gray diamonds indicate blood T$_{EM}$ from healthy donors and black diamonds indicate paired blood T$_{EM}$ of patients. T$_{EM}$, effector memory T cell; T$_M$, memory T cell; T$_N$, naive T cell; T$_{RM}$, resident memory T cell.

CD103$^+$ T$_{RM}$ when compared with circulating T cells. The role of EGR2 in lung T$_{RM}$ regulation was previously demonstrated in influenza mouse models, in which T-cell-specific deletion of EGR2 reduced the numbers of lung CD8$^+$ T$_{RM}$ and impaired lung CD4$^+$ T-cell responses.[46] CD103$^+$ T$_{RM}$ also expressed high transcript levels of *Notch1*, a direct

target of EGR2 (ref. 46) (**Figure 4d**). Furthermore, increased transcript levels were observed for the transcriptional regulator *RBPJ*, central to Notch signaling, and the Notch ligand *JAG2* (**Figure 4d**). Moreover, we found increased expression of *ZEB2*, encoding a transcription factor regulated by Notch signaling in mice.[47]
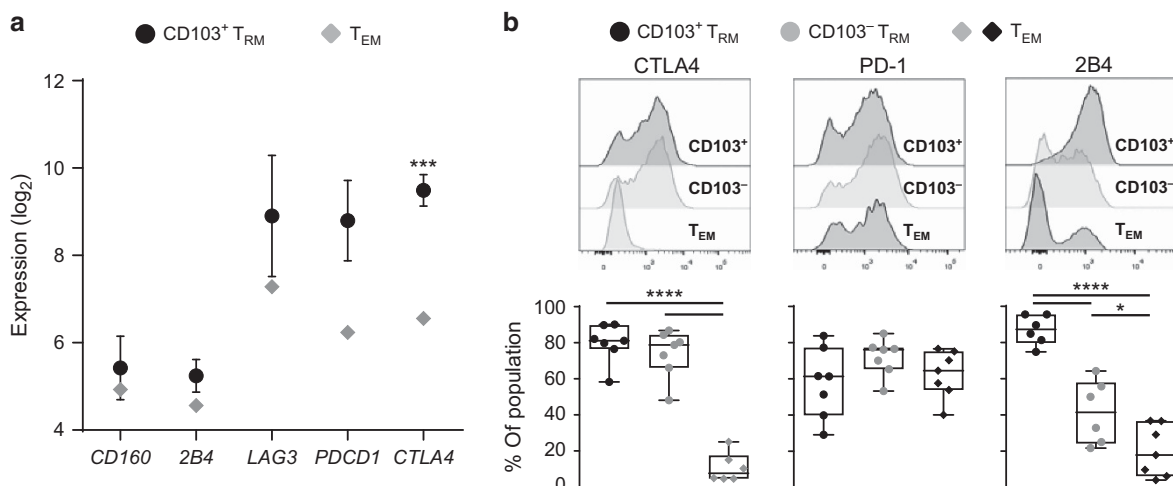
Figure 5 Lung CD4$^+$ T$_{RM}$ express inhibitory checkpoint receptors. (**a**) The expression of genes encoding inhibitory checkpoint molecules by lung CD103$^+$ T$_{RM}$ (black circles) and blood T$_{EM}$ (gray diamonds) was analyzed. (**b**) The protein expression of CTLA4, PD-1, and 2B4 was determined for lung CD103$^+$ T$_{RM}$ (black circles), CD103$^-$ T$_{RM}$ (gray circles), and blood T$_{EM}$ (gray or black diamonds) and is shown by representative histogram overlay and quantification of percentage of the population. (**a**) The y axes show log$_2$-transformed normalized values. Each symbol depicts the mean ($\pm$ s.d.). ***False-discovery rate (FDR) < 0.001. For the blood samples, five individually sorted samples were pooled before the microarray analysis. (**b**) The quantifications are shown as box–whisker plots with min–max. Each symbol depicts an individual sample; horizontal line shows the median; $n = 7$. *$P < 0.05$ and ****$P < 0.0001$; 1-way analysis of variance ANOVA with Holm–Sidak multiple comparison test. (**a**,**b**) For the blood subsets, gray diamonds indicate blood T$_{EM}$ from healthy donors and black diamonds indicate paired blood T$_{EM}$ of patients. T$_{EM}$, effector memory T cell; T$_{RM}$, resident memory T cell.

To experimentally address the potential role of Notch in the regulation of CD4$^+$ T$_{RM}$, we analyzed the CD4$^+$ T$_{RM}$ composition in the lungs of steady-state *RBPJ*$^{fl/fl}$*Cd4-Cre*$^+$ (RBPJ knockout (KO)) mice and *RBPJ*$^{fl/fl}$*Cd4-Cre*$^+$ wild-type littermates. We found lower frequencies of CD4$^+$CD103$^+$ T$_{RM}$ in the RBPJ KO mice (**Figure 4e**) suggesting that Notch plays a role in the formation or maintenance of CD4$^+$CD103$^+$ T$_{RM}$. Overall, we identified a unique set of transcription factors that may regulate CD4$^+$CD103$^+$ T$_{RM}$, including several transcriptional regulators of effector function.

Lung CD4$^+$ T$_{RM}$ express several inhibitory receptors
To explore the functional properties of the CD4$^+$CD103$^+$ T$_{RM}$ we determined the expression of inhibitory molecules often associated with T-cell exhaustion. CD4$^+$CD103$^+$ T$_{RM}$ expressed a variety of inhibitory checkpoint molecules, such as *PDCD1* (encoding for PD-1), *CTLA4*, and *LAG3* (**Figure 5a**). Protein expression was confirmed for PD-1 and CTLA4 and although we did not find 2B4 (CD244) to be differentially expressed at mRNA level, all CD4$^+$CD103$^+$ T$_{RM}$ expressed high 2B4 protein, whereas only a portion of circulating T$_{EM}$ did (**Figure 5b**). The geometric mean fluorescence intensity for PD-1 was not increased in the CD4$^+$CD103$^+$ T$_{RM}$ either (**Supplementary Figure S4a**). To assess whether the disease state affects the expression of PD-1 on blood T$_{EM}$, we determined the expression in a cohort of healthy age-matched donors. Similar PD-1 levels were observed between patient and donor blood T$_{EM}$ (**Supplementary Figure S4b**). This suggests that the T$_{RM}$ are chronically or intermittently activated and thus potentially exhausted. Therefore, next we investigated the responsiveness of these cells *in vitro*.

Lung CD4$^+$CD103$^+$ T$_{RM}$ exhibit rapid and polyfunctional cytokine responses
Ideally T$_{RM}$ should be poised for rapid effector function upon activation as they are perceived as part of the first line of defense upon secondary infections. To investigate this role in lung CD4$^+$CD103$^+$ T$_{RM}$, we analyzed the transcript levels of various chemokines and effector molecules. Relative to blood-derived T$_{EM}$, lung CD4$^+$CD103$^+$ T$_{RM}$ expressed high transcript levels for genes encoding for several chemokines and cytotoxic molecules (**Figure 6a**). We found differentially high expression of *CCL4*, *CXCL16*, and *XCL1* and similar trends for *CCL3*, *CCL5*, and *CCL18*. These elevated mRNA levels may serve to allow rapid translation and secretion to attract and position auxiliary immune cells, a key function of T$_{RM}$, following infection.[5,48,49] The high expression of *CXCL16* may be of special interest as its receptor (CXCR6) was found to be highly expressed on lung CD8$^+$ T$_{RM}$.[13] High expression of *XCL1* was also described for lung CD8$^+$ T$_{RM}$[13] and is shown to mediate cytotoxic immune function.[50,51]

Effector and cytotoxic molecules for which transcript levels were elevated in CD4$^+$CD103$^+$ T$_{RM}$ include *IFNG*, *GZMA*, *GZMB*, and *PRF1* (**Figure 6a**). Such deployment-ready mRNA suggests an alert state and readiness to respond to incoming pathogens and prevent the spreading of infections. Indeed, when activated with αCD3/αCD28, CD4$^+$CD103$^+$ T$_{RM}$ demonstrated accelerated kinetics for IFNγ production when compared with blood-derived CD45RA$^-$ memory T-cells (T$_M$) (**Figure 6b**). Although after only 2 h of stimulation, on average 17% of CD4$^+$CD103$^+$ T$_{RM}$ produced IFNγ, most blood-derived cells did not accumulate IFNγ protein. Similar responses were observed for tumor necrosis factor-α
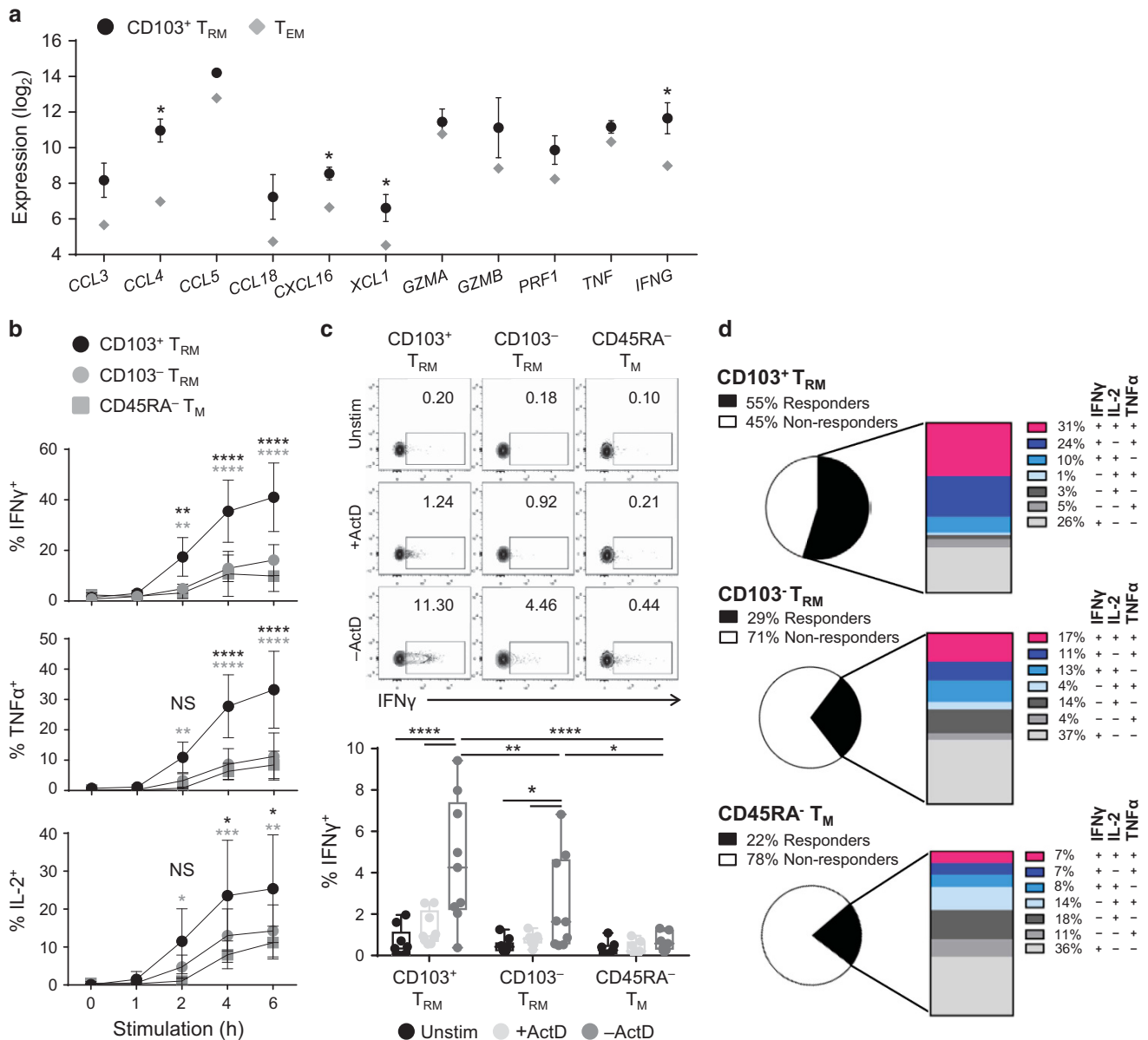
Figure 6 Lung CD103$^+$ T$_{RM}$ are polyfunctional. (**a**) The expression of genes encoding chemokines and effector molecules by CD103$^+$ T$_{RM}$ (black circle) and blood T$_{EM}$ (gray diamonds). (**b**) Frequency of IFNγ$^+$, TNFα$^+$, and IL-2$^+$ cells in CD103$^+$ T$_{RM}$ (black circles), CD103$^-$ T$_{RM}$ (gray circles), and blood CD45RA$^-$ T$_M$ (gray squares) was measured after 0, 1, 2, 4, and 6 h of αCD3/αCD28 stimulation in the presence of Brefeldin A. (**c**) Frequency of IFNγ$^+$ cells of CD103$^+$ T$_{RM}$, CD103$^-$ T$_{RM}$, and blood CD45RA$^-$ T$_M$ was determined 2 h after αCD3/αCD28 stimulation with (light gray) or without Actinomycin D (ActD) (dark gray) or unstimulated (black), all in the presence of Brefeldin A. Top panels show representative contour plots and frequencies are quantified as percentage of the population below. (**d**) The polyfunctionality of CD103$^+$ T$_{RM}$, CD103$^-$ T$_{RM}$, and blood CD45RA$^-$ T$_M$ was quantified. The pie charts show the frequency of responders (cells producing ≥ 1 of the cytokines, interferon-γ (IFNγ), tumor necrosis factor-α (TNFα), or interleukin-2 (IL-2)). From the responders, the rectangle shows the frequency of cells producing all 3 cytokines (pink), 2/3 cytokines (shades of blue), or 1/3 cytokines (shades of gray). (**a**) The y axes show log$_2$-transformed normalized values. Each symbol depicts the mean ($\pm$ s.d.). *False-discovery rate (FDR) < 0.05; $n = 5$ for lung samples. For the blood samples, five individually sorted samples were pooled before the microarray analysis. (**b**) Each symbol depicts the mean ($\pm$ s.d.); $n = 5$. *$P < 0.05$, **$P < 0.01$, ***$P < 0.001$, and ****$P < 0.0001$; 2-way analysis of variance (ANOVA) with Tukey's multiple comparisons test. Significance is shown for the comparison of the CD103$^+$ T$_{RM}$ to CD103$^-$ T$_{RM}$ (black stars) and to blood CD45RA$^-$ T$_M$ (gray stars) for the different time points. (**c**) The quantifications are shown as box–whisker plots with min–max. Each symbol depicts an individual sample; horizontal line shows the median; $n = 7$–9. *$P < 0.05$, **$P < 0.01$, and ****$P < 0.0001$; 2-way ANOVA with Tukey's multiple comparison test. (**d**) The bar graphs show the mean values; $n = 5$. (**a–d**) Blood from healthy donors. T$_{EM}$, effector memory T cell; T$_M$, memory T cell; T$_{RM}$, resident memory T cell.

and interleukin-2. After 6 h of stimulation, not only more CD103$^+$ T$_{RM}$ produced IFNγ, interleukin-2, and tumor necrosis factor-α when compared with blood CD45RA$^-$ T$_M$, but also more effector molecules per cell were detected for IFNγ (geometric mean fluorescence intensity; **Supplementary**

Figure S5a). In contrast, lung CD103$^-$ T$_{RM}$ demonstrated relatively similar effector cytokine expression as blood CD45RA$^-$ T$_M$ upon T-cell receptor stimulation.

As the CD103$^+$ T$_{RM}$ constitutively expressed high IFNγ transcript and rapidly produced copious amounts of IFNγ

protein, we set out to investigate whether the preformed transcript provides the T_{RM} with a kick start. To do so, we pretreated lung and blood T cells with Actinomycin D (ActD), blocking *de novo* transcription, followed by T-cell receptor stimulation. In this way the protein produced has to be derived from the preformed transcript. After 2 h of stimulation, the non-ActD-treated CD103$^+$ T_{RM} produced IFNγ, whereas the ActD-treated CD103$^+$ T_{RM} produced significantly less (**Figure 6c**). Thus, the T_{RM} appear to mainly rely on *de novo* transcription for their superior cytokine production.

Potency of effector T-cell function is defined as the ability to produce multiple cytokines simultaneously. This polyfunctionality is gradually lost upon T-cell exhaustion.[52,53] We calculated the percentage of cells that produced at least one cytokine, referred to as the responders (**Figure 6d**). As such, the percentage of responders among CD103$^+$ T_{RM} cells was 55%, more than twice as high as the percentage of responders among the blood-derived memory T cells. The percentage of polyfunctional responders was significantly higher in the CD103$^+$ T_{RM} population (31%) when compared with blood CD45RA$^-$ T_M (7%) (**Figure 6d** and **Supplementary Figure S5b**). In summary, we showed that although CD4$^+$CD103$^+$ T_{RM} expressed several inhibitory molecules associated with T-cell exhaustion, these cells were more than capable of rapidly producing a multitude of cytokines upon stimulation and thus do not correspond with their "exhausted" phenotype.

DISCUSSION

Here we analyzed the molecular and functional profiles of the previously uncharacterized, but abundantly present, CD4$^+$ T_{RM} population in the human lungs. We addressed several properties of CD4$^+$ T_{RM} demonstrating their adaptation to the tissue niche, including the expression of a wide range of chemokine receptors and adhesion molecules and a strictly controlled effector mechanism designed to effectively mediate pathogen control while safeguarding the fragile lung environment. T_{RM} are traditionally defined by the expression of CD103 and CD69, the latter molecule blocking tissue egress by the inhibition of S1PR1 function.[21] Recently, these criteria have been challenged, as CD69$^+$ cells were found to recirculate[31] and CD69$^-$ cells were found to be resident.[54] In support of this, we demonstrated that lung CD4$^+$CD69$^-$ T cells are composed of effector and memory cells, whereas circulating CD4$^+$ T cells mainly consist of naive and central memory T cells. Thus the CD4$^+$CD69$^-$ T cells are not in strict equilibrium with circulating CD4$^+$ T cells. The characterization of T_{RM} by the expression of CD103 remains undisputed, as this molecule is important to dock T cells to the epithelial E-cadherin.[22,23,55,56] We therefore identified lung CD4$^+$ T_{RM} cells by the expression of CD103 and found these cells to clearly express a distinct mRNA expression profile when compared with circulating CD4$^+$ T cells. Using classical flow cytometric analysis, we showed that at least three different lung CD4$^+$ T-cell subsets could be established based on the expression of CD69 and CD103. More detailed phenotyping revealed a previously unrecognized complexity of the CD4$^+$ T_{RM} compartment in

the lung. For example, the expression of VLA-1, CXCR6, and even inhibitory molecules, such as 2B4, did not strictly associate to any of the three populations as addressed by the conventional phenotyping method. Future single-cell approaches may deal with this caveat of population-averaged measurements in conventional transcriptome analysis experiments.

A large body of evidence indicates the indispensable role of CD8$^+$ and CD4$^+$ T_{RM} in protecting the lung against respiratory pathogens.[1,2,10,11,42,57] For this purpose, T_{RM} must be equipped to immediately react when a pathogen enters the lungs. However, such responses need to be kept in check, as excessive cytotoxicity may damage the fragile lung architecture and compromise its vital function. We previously published that human CD8$^+$ T_{RM} are specifically programmed for this tightly regulated effector function.[13] In line with this, others have shown that when lung T_{RM} function is not effectively controlled there is an increased correlation with inflammatory diseases of the airway, such as asthma.[58] Here, we describe that similar mechanisms may apply to the lung CD4$^+$ T_{RM} compartment, as we found a high degree of resemblance of differentially expressed genes that regulate T-cell effector function between the CD8$^+$ and CD4$^+$ T_{RM}. This suggests that the lung environment is important for the transcriptional and functional identity of lung T_{RM}, regardless of their lineage. CD4$^+$CD103$^+$ T_{RM} also constitutively expressed mRNA for various effector molecules potentially underlying the rapid response to T-cell receptor stimulation. In addition, we demonstrated that not only the magnitude, but also the quality of the effector response is different when compared with blood T cells, as the T_{RM} exhibited a higher degree of polyfunctionality. Although CD4$^+$CD103$^+$ T_{RM} showed elevated transcript levels of IFNγ, suggesting that the rapid production of IFNγ is due to the lack of transcriptional delay, our data suggest that this is not entirely the case. We showed that CD4$^+$CD103$^+$ T_{RM} require active transcription to produce effector cytokines, as the cytokine production was diminished upon blockade of *de novo* transcription. This rather proposes that the IFNγ locus is readily accessible in the T_{RM}. Simultaneously, the T_{RM} do not produce IFNγ protein until stimulated, indicating that the T_{RM} are poised for effector function. This may be elementary to the core tasks of CD4$^+$ T_{RM}, as IFNγ is essential for the swift recruitment of auxiliary immune cells to the site of infection,[49,59] protection against respiratory viruses,[57] as well as the formation of CD8$^+$CD103$^+$ T_{RM} in the lung.[5] At the same time, although rapid effector function of T_{RM} is desirable when combating incoming pathogens, release of effector molecules needs stringent regulation to prevent excessive immunopathology to the fragile lung tissue. Next to the strict translational control, as a second potential safety mechanism, CD4$^+$ T_{RM} expressed high levels of various inhibitory checkpoint molecules. It is likely that *in vivo* these inhibitory molecules depend on their ligands to limit activation of the CD4$^+$ T_{RM}. Controversially, such receptors indicate chronic or intermittent activation and therefore potential exhaustion, especially in the context of tumor tissues.[60] As lung CD4$^+$CD103$^+$ T_{RM} possessed the capacity to robustly and polyfunctionally respond

to T-cell receptor stimulation, our data provide more insights regarding T-cell exhaustion. Furthermore, it indicates that tissue context should be considered when interpreting T-cell dysfunction on the basis of checkpoint molecule expression.

A large proportion of the CD4$^+$ T cells in the lungs expressed the chemokine receptor CXCR6. As lung epithelial cells constitutively express the CXCR6 ligand CXCL16, this axis may be crucial for homing of T cells to the lung tissue.[61] This mechanism may also be more generic, as liver-resident natural killer (NK) and NK T cells, as well as lymphoid tissue-derived NK cells express CXCR6.[62–64] In addition, CD4$^+$ T$_{RM}$ populations uniformly expressed CXCR3 and CCR5, the chemokine receptors that are important for T-cell recruitment to inflamed lungs.[39–41] CXCR3 is also more broadly described to regulate T-cell recruitment to sites of inflammation or disease.[65–69] The preferential expression of the integrin VLA-1 by CD4$^+$CD103$^+$ T$_{RM}$ could account for their survival and accumulation in the vicinity of the lung epithelium, as was previously shown for mouse CD8$^+$ and CD4$^+$ T$_{RM}$.[34,70] Simultaneously, VLA-1 expression discriminates CD8$^+$ T$_{RM}$ with high cytotoxic potential specifically localized in the epidermis of human skin.[71] We have previously shown that CD8$^+$CD103$^+$ T$_{RM}$ line the epithelium of the human lung.[72] It has recently been shown that CD4$^+$ and CD8$^+$ T$_{RM}$ localize differently in the lungs of mice. CD4$^+$ T$_{RM}$ cluster in bronchus-associated lymphoid tissue structures, whereas CD8$^+$ T$_{RM}$ form niches around areas of tissue damage.[73] Similar structures were observed in the skin, female reproductive tract, and intestines.[31,74,75] As to whether similar clusters exist in the human lungs needs further investigation.

Recently, we demonstrated that Notch signaling is required for the maintenance of lung CD8$^+$CD103$^+$ T$_{RM}$.[13] More recently, similar Notch signatures were identified in CD8$^+$ T cell with T$_{RM}$ like features in lung cancer.[76] Our data suggest that Notch may play a similar role in the regulation of lung CD4$^+$ T$_{RM}$. Moreover, the immunomodulatory role of Notch signaling in the lungs may not be restricted to T cells, as other studies demonstrated Notch dependency of lung dendritic cells and macrophages.[77,78] Notch is a surface receptor that, upon stimulation by Delta-like ligands, acts as a transcriptional activator.[79] Consequently, tissue environmental-induced Notch signaling can directly lead to expression of mRNA encoding for Notch target genes, including IFNγ.[80] This type of mechanism demonstrates the perfect adaption of T$_{RM}$ to the lung environment. In addition, as pharmaceutical inhibitors of Notch signaling are available, this offers ways for therapeutic intervention when T$_{RM}$ mediate pathology in the airways.

CD4$^+$ T$_{RM}$ expressed low to intermediate levels of T-bet and Eomes. The downregulation of these two transcription factors is necessary for the formation of CD8$^+$ T$_{RM}$, and thus similar mechanisms may be important for CD4$^+$ T$_{RM}$. Strikingly, we did not detect protein expression of the Hobit (encoded by ZNF683) transcription factor that serves as an ontogenic regulator of T$_{RM}$ formation.[43] These results appear counter-intuitive, as we found CD4$^+$CD103$^+$ T$_{RM}$ to express high mRNA levels encoding for this transcription factor that is in contrast to our previous findings in circulating T cells.[44,81] Our data do not exclude a possible role of Hobit for the formation of human lung CD4$^+$ T$_{RM}$ and as its expression was found to be regulated by stimulation in NKT cells,[82] more research is required.

Overall, our work strengthens the fundamental understanding of CD4$^+$ T cells residing in the human lungs. This knowledge will create opportunities for novel therapeutic manipulation of CD4$^+$ T$_{RM}$ in terms of vaccine design and immunotherapy. Ideally, these cells could be harnessed to boost the efficacy of vaccine regimens. In addition, as T$_{RM}$ can also contribute to local pathology,[58] identifying novel targets can enable selective deletion of these cells for therapeutic intervention.

METHODS

Subjects. Lung tissue samples were obtained from a total of 85 patients with an average age of 63.9 years. In all, 70 patients underwent lobectomy for a peripheral primary lung tumor and 15 received a lung transplantation due to end-stage pulmonary disease. The exclusion criteria included history of asthma or a recent lower respiratory tract infection. The patients did not receive systemic immunosuppressive drugs, chemotherapy, or radiotherapy. Lung material from six lobectomy patients was used for the microarray, of whom two had normal lung function and four had mild to moderate chronic obstructive pulmonary disease. For the other assays samples were chosen at random. The lobectomy patients were recruited from the Academic Medical Centre (AMC), Amsterdam, The Netherlands, Tergooi Hospitals, Hilversum, The Netherlands, and Onze Lieve Vrouwe Gasthuis (OLVG), Amsterdam, The Netherlands, and the transplantation patients were recruited from University Medical Centre Groningen, Groningen, The Netherlands. Sanquin Blood Supply Foundation, Amsterdam, The Netherlands, supplied the buffy coats of donors used as healthy controls. The age and sex of the healthy donors is unknown.

Mice. *RBPJ$^{fl/fl}$Cd4-Cre$^+$* (RBPJ KO) and *RBPJ$^{fl/fl}$Cd4-Cre$^-$* (wild-type) littermates on C57BL/6/NCrl background were bred and housed in pathogen-free conditions at the Animal Resources Center of the AMC (Amsterdam, The Netherlands). The mice were males and females between 8 and 29 weeks old.

Study approval. Written informed consent was given by all of the patients and donors before inclusion into the study. The ethical review board of the AMC and the METC/CCMO of the OLVG approved the study under the MEC-U number NL52453.100.15 according to the Declaration of Helsinki. All mice were used in accordance of institutional and national animal experimentation guidelines.

Isolation of mononuclear cells from peripheral blood and lung tissue. Peripheral blood mononuclear cells were isolated from heparinized peripheral blood samples with standard density gradient techniques. For the lung material, after the lobectomy the pathologist cuts off a piece of peripheral normal-looking lung tissue farthest away from the tumor. The lung mononuclear cells were isolated from the tissue as previously described.[4,83] In short, the tissue was sliced into 1 mm pieces using a McIlwain tissue chopper (Loughborough, UK) and incubated at 37 °C in digestion medium (RPMI with 20 mM Hepes, 15% fetal calf serum, and 50 U ml^{-1} DNAse type I (Sigma-Aldrich, Zwijndrecht, the Netherlands)). The tissue pieces were dried with sterile gauze and incubated for 60 min with medium and collagenase type I or 4 (300 U ml^{-1}; Worthington, The Hague, the Netherlands) at 37 °C while shaking. The digested tissue was passed through a flow-through chamber to achieve a cell suspension. To isolate mononuclear cells from the cell suspension, standard density gradient techniques

were used. The lung mononuclear cell and peripheral blood mononuclear cell samples were cryopreserved in liquid nitrogen until further analysis.

Lungs of the mice were cut into small pieces and digested with Collagen type I (750 U ml^{-1}; Gibco, Landsmeer, the Netherlands) and DNAse type I (0.31 mg ml^{-1}; Roche, Woerden, the Netherlands) in Iscove's modified Dulbecco's medium for 30 min at 37 °C, followed by filtration. To isolate mononuclear cells from the cell suspension, standard density gradient techniques were used.

Flow cytometric cell sorting. For gene expression analysis, peripheral blood mononuclear cells and lung mononuclear cells were sorted based on different combinations of the following antibodies: CD27, CD45RO, CD103, CD45RA, CD3, CD8, CD4, and CD69.

RNA isolation, amplification, labeling, and hybridization. RNA from the sorted cells was isolated using the Nucleospin RNA XS and Nucleospin RNA II kit (Macherey-Nagel) in accordance with the manufacturer's protocols. Amplification, labeling, hybridization, and data extraction were done by ServiceXS (Leiden, The Netherlands). Hybridization was performed on to Whole Human Genome HT12-Microarrays (Illumina, Leiden, the Netherlands) and the Illumina iScan array scanner was used to scan the arrays. Illumina GenomeStudio v2011.1 software was used to retrieve the data. Because of low average signal after the hybridization, four of the microarrays were excluded.

Microarray analysis. Analyses were carried out with packages from Bioconductor in the statistical software package R (version 3.0.0, Auckland, New Zealand). Normexp-by-control background correction, quantile normalization, and log$_2$ transformation[84] were performed on the Illumina sample and control probe profiles using the limma package (version 3.16.8). Using the arrayQualityMetrics package (version 3.16.0, Bioconductor Buffalo, NY) one outlier array was detected. This array was discarded and the data were renormalized. Technical replicate arrays were averaged. Only probes detected (detection P value < 0.05) on at least one array were included in the differential expression analysis. Gene-wise linear models were fitted using the limma package. A consensus intrapatient correlation was estimated for measurements on the same subject (function 'duplicateCorrelation', package limma) and included in the linear model fit. Differential gene expression between the different conditions was assessed via a moderated t-test. Resulting P values were corrected for multiple testing using the Benjamini–Hochberg false discovery rate. The illuminaHumanv4.db package (version 1.18.0) was used to update the probe annotation provided by Illumina. The microarray data have been deposited in the NCBI (National Center for Biotechnology Information) Gene Expression Omnibus (GEO) in a MIAME compliant format and are accessible under GEO Series accession number GSE103527.

Quantitative PCR. For validation of the microarray data, RNA was isolated from the sorted samples using Invisorb RNA isolation kit (Invitek, Berlin, Germany) or Trizol reagent (Invitrogen, Landsmeer, the Netherlands). Complementary DNA was synthesized using RevertAID H Minus Reverse Transcriptase (Thermo Scientific, Landsmeer, the Netherlands) and random primers (Invitrogen) or poly dT oligos (Invitrogen). Quantitative PCR analysis was performed in duplicate using Power SYBR Green (Applied Biosystem, Landsmeer, the Netherlands) with StepOnePlus Real-Time PCR system (Applied Biosystem). The gene expression was normalized to S18. The primers used are listed in **Supplementary Table S3**.

Flow cytometry analysis. Human peripheral blood mononuclear cells or lung mononuclear cells were labeled with combinations of the following antibodies: anti-CD4, anti-CD3, anti-CD8, anti-CD27, anti-CD45RA, anti-CD69, anti-CD103, anti-CD49a, anti-CXCR6, anti-CXCR3, anti-CCR5, anti-CD28, anti-CCR7, anti-PD-1, and anti-2B4. Near-infrared fixable dye (Invitrogen) was used to exclude dead cells

from the analysis. For intracellular staining the following antibodies were used: anti-CTLA4, anti-Hobit, anti-Eomes, anti-T-bet, anti-IFNγ, anti-interleukin-2, and anti-tumor necrosis factor-α. To stain for Hobit a labeled secondary anti-IgM was used. The cells were labeled according to the manufacturer's instructions. For the intracellular staining the cells with fixed and permeabilized using the Foxp3/Transcription Factor Staining kit (eBioscience, Landsmeer, the Netherlands). For analysis of the mouse T$_{RM}$, the lung cells were stained with the following fluorochrome-conjugated antibodies: anti-CD3, anti-CD4, anti-CD44, anti-CD62L, anti-CD103, anti-CD69, and CD1d tetramer at 4 °C for 30 min. Near-infrared fixable dye (Invitrogen) was used to exclude dead cells from the analysis. The cells were labeled according to the manufacturer's instructions. For the intracellular staining with Foxp3, cells were fixed and permeabilized using the Foxp3/Transcription Factor Staining kit (eBioscience). All samples were measured in phosphate-buffered saline 0.5% fetal calf serum with a LSR Fortessa (BD, Temse, Belgium) and the analysis was performed using FlowJo Version 10 software (Temse, Belgium). See **Supplementary Table S4** for the full list of antibodies used in this paper.

In vitro stimulation assays. Cytokine production by the CD4$^+$ T cells was determined by incubating the cells with plate-bound αCD3 (HIT3A; eBioscience) and soluble CD28 (s.28; CLB, De Rijp, the Netherlands) for 6 h at 37 °C in the presence of Brefeldin A (eBioscience). For the experiments using ActD, CD4$^+$ T cells were isolated using MACS (Miltenyi Biotec, Leiden, the Netherlands). Where indicated, T cells were pretreated with ActD (Sigma-Aldrich) for 30 min at 37 °C before activation with plate-bound αCD3 (HIT3A; eBioscience) and soluble CD28 (s.28; CLB) for 2 h at 37 °C in the presence of Brefeldin A (eBioscience).

Statistics. To determine the significance of our flow cytometry results we used one-way analysis of variance and Holm–Sidak multiple comparisons test using GraphPad Prism 6 (La Jolla, CA). To analyze the significant of the mouse T$_{RM}$, paired T-test was used. Two-way analysis of variance and Tukey's multiple comparisons test was used to determine the significance of the in vitro functional assays. The P value of < 0.05 was considered statistically significant (*P < 0.05; **P < 0.01; ***P < 0.001; ****P < 0.0001). Gene-E v3.0.206 (Cambridge, MA) was used to make the heat maps for which the mean and maximum values for each row was used to generate the heat map colors.

AUTHOR CONTRIBUTIONS
A.E.O., B.P., M.A.N., R.A.W.v.L., and P.H. designed the project and experiments. A.E.O., B.P., C.H., R.E.J., R.S., D.v.d.Z., H.B., E.B.M.R., and P.H. performed the experiments and/or collected the tissue and blood samples. All authors contributed to the interpretation and discussion of the data. A.E.O., R.A.W.v.L., and P.H. wrote the manuscript. All authors read and approved the manuscript.

DISCLOSURE
The authors declared no conflict of interest.

REFERENCES
1. Teijaro, J.R., Verhoeven, D., Page, C.A., Turner, D. & Farber, D.L. Memory CD4 T cells direct protective responses to influenza virus in the lungs through helper-independent mechanisms. *J. Virol.* **84**, 9217–9226 (2010).

2. Teijaro, J.R. et al. Cutting edge: Tissue-retentive lung memory CD4 T cells mediate optimal protection to respiratory virus infection. *J. Immunol.* **187**, 5510–5514 (2011).

3. Mckinstry, K.K. et al. Memory CD4 + T cells protect against influenza through multiple synergizing mechanisms. *J. Clin. Invest.* **122**, 2847–2856 (2012).

4. Sathaliyawala, T. et al. Distribution and compartmentalization of human circulating and tissue-resident memory T cell subsets. *Immunity* **38**, 187–197 (2013).

5. Laidlaw, B.J. et al. CD4 + T cell help guides formation of CD103 + lung-resident memory CD8 + T cells during influenza viral infection. *Immunity* **41**, 633–645 (2014).

6. Sallusto, F., Lenig, D., Förster, R., Lipp, M. & Lanzavecchia, A. Two subsets of memory T lymphocytes with distinct homing potentials and effector functions. *Nature* **401**, 708–712 (1999).

7. Mueller, S.N., Gebhardt, T., Carbone, F.R. & Heath, W.R. Memory T cell subsets, migration patterns, and tissue residence. *Annu. Rev. Immunol.* **31**, 137–161 (2013).

8. Bevan, M.J. Memory T cells as an occupying force. *Eur. J. Immunol.* **41**, 1192–1195 (2011).

9. Park, C.O. & Kupper, T.S. The emerging role of resident memory T cells in protective immunity and inflammatory disease. *Nat. Med* **21**, 688–697 (2015).

10. Turner, D.L. et al. Lung niches for the generation and maintenance of tissue-resident memory T cells. *Mucosal Immunol.* **7**, 501–510 (2014).

11. Wu, T. et al. Lung-resident memory CD8 T cells (TRM) are indispensable for optimal cross-protection against pulmonary virus infection. *J. Leukoc. Biol.* **95**, 215–224 (2014).

12. Lee, Y.-N., Lee, Y.-T., Kim, M.-C., Gewirtz, A.T. & Kang, S.-M. A novel vaccination strategy mediating the induction of lung-resident memory CD8 T cells confers heterosubtypic immunity against future pandemic influenza virus. *J. Immunol.* **196**, 2637–2645 (2016).

13. Hombrink, P. et al. Programs for the persistence, vigilance and control of human CD8 + lung-resident memory T cells. *Nat. Immunol.* **17**, 1467–1478 (2016).

14. Wakim, L.M. et al. The molecular signature of tissue resident memory CD8 T cells isolated from the brain. *J. Immunol.* **189**, 3462–3471 (2012).

15. Steinbach, K. et al. Brain-resident memory T cells represent an autonomous cytotoxic barrier to viral infection. *J. Exp. Med.* **213**, 1571–1587 (2016).

16. Watanabe, R. et al. Human skin is protected by four functionally and phenotypically discrete populations of resident and recirculating memory T cells. *Sci. Transl. Med.* **7**, 279ra39 (2015).

17. Glennie, N.D. et al. Skin-resident memory CD4 + T cells enhance protection against Leishmania major infection. *J. Exp. Med.* **212**, 1405–1414 (2015).

18. Shin, H. & Iwasaki, A. A vaccine strategy that protects against genital herpes by establishing local memory T cells. *Nature* **491**, 463–467 (2012).

19. Mackay, L.K. et al. Long-lived epithelial immunity by tissue-resident memory T (T RM) cells in the absence of persisting local antigen presentation. *Proc. Natl. Acad. Sci. USA* **109**, 7037–7042 (2012).

20. Kinzler, K.W. et al. GRK2-dependent S1PR1 desensitization. *Science* **333**, 1898–1903 (2011).

21. Skon, C.N. et al. Transcriptional downregulation of S1pr1 is required for the establishment of resident memory CD8 + T cells. *Nat. Publ. Gr.* **14**, 1285–1293 (2013).

22. Casey, K.A. et al. Antigen-independent differentiation and maintenance of effector-like resident memory T cells in tissues. *J. Immunol.* **188**, 4866–4875 (2012).

23. Cepek, K.L. et al. Adhesion between epithelial cells and T lymphocytes mediated by E-cadherin and the alpha E beta 7 integrin. *Nature* **372**, 190–193 (1994).

24. Nakayamada, S., Takahashi, H., Kanno, Y. & O'Shea, J.J. Helper T cell diversity and plasticity. *Curr. Opin. Immunol.* **24**, 297–302 (2012).

25. Boyce, J.A. et al. Mechanisms of allergic diseases mechanisms underlying helper T-cell plasticity: implications for immune-mediated disease. *J. Allergy Clin. Immunol.* **131**, 1276–1287 (2013).

26. Crotty, S. Follicular helper CD4 T cells (T FH). *Annu. Rev. Immunol.* **29**, 621–663 (2011).

27. Schmitt, N. & Ueno, H. Regulation of human helper T cell subset differentiation by cytokines. *Curr. Opin. Immunol.* **34**, 130–136 (2015).

28. Becattini, S. et al. Pathogens or Vaccines. *Science (80-.)* **347**, 400–406 (2015).

29. Swain, S.L., McKinstry, K.K. & Strutt, T.M. Expanding roles for CD4 + T cells in immunity to viruses. *Nat. Rev. Immunol.* **12**, 136–148 (2012).

30. Bromley, S.K., Yan, S., Tomura, M., Kanagawa, O. & Luster, A.D. Recirculating memory T cells are a unique subset of CD4 + T cells with a distinct phenotype and migratory pattern. *J. Immunol.* **190**, 970–976 (2013).

31. Collins, N. et al. Skin CD4(+) memory T cells exhibit combined cluster-mediated retention and equilibration with the circulation. *Nat. Commun.* **7**, 11514 (2016).

32. Pan, Y. et al. Survival of tissue-resident memory T cells requires exogenous lipid uptake and metabolism. *Nature* **543**, 252–256 (2017).

33. Richter, M. et al. Collagen distribution and expression of collagen-binding 1 1 (VLA-1) and 2 1 (VLA-2) integrins on CD4 and CD8 T cells during influenza infection. *J. Immunol.* **178**, 4506–4516 (2007).

34. Chapman, T.J. & Topham, D.J. Identification of a unique population of tissue-memory CD4 + T cells in the airways after influenza infection that is dependent on the integrin VLA-1. *J. Immunol.* **184**, 3841–3849 (2010).

35. Denucci, C.C., Mitchell, J.S. & Shimizu, Y. Integrin function in T-cell homing to lymphoid and nonlymphoid sites: getting there and staying there. *Crit. Rev. Immunol.* **29**, 87–109 (2009).

36. Mueller, S.N. & Mackay, L.K. Tissue-resident memory T cells: local specialists in immune defence. *Nat. Publ. Gr.* **16**, 79–89 (2015).

37. Raine, T., Liu, J.Z., Anderson, C.A., Parkes, M. & Kaser, A. Generation of primary human intestinal T cell transcriptomes reveals differential expression at genetic risk loci for immune-mediated disease. *Gut* **64**, 250–259 (2015).

38. von Andrian, U.H. & Mempel, T.R. Homing and cellular traffic in lymph nodes. *Nat. Rev. Immunol.* **3**, 867–878 (2003).

39. Thomas, S.Y., Banerji, A., Medoff, B.D., Lilly, C.M. & Luster, A.D. Multiple chemokine receptors, including CCR6 and CXCR3, regulate antigen-induced T cell homing to the human asthmatic airway. *J. Immunol.* **179**, 1901–1912 (2007).

40. Kohlmeier, J.E. et al. CXCR3 directs antigen-specific effector CD4 + T cell migration to the lung during parainfluenza virus infection. *J. Immunol.* **183**, 4378–4384 (2009).

41. Kohlmeier, J.E. et al. The chemokine receptor CCR5 plays a key role in the early memory CD8 + T cell response to respiratory virus infections. *Immunity* **29**, 101–113 (2008).

42. Mackay, L.K. et al. T-box transcription factors combine with the cytokines TGF-β and IL-15 to control tissue-resident memory T cell fate. *Immunity* **43**, 1101–1111 (2015).

43. Mackay, L.K. et al. Hobit and Blimp1 instruct a universal transcriptional program of tissue residency in lymphocytes. *Science* **352**, 459–463 (2016).

44. Oja, A.E. et al. The transcription factor hobit identifies human cytotoxic CD4 + T cells. *Front. Immunol.* **8**, 1–11 (2017).

45. Vasanthakumar, A. et al. The transcriptional regulators IRF4, BATF and IL-33 orchestrate development and maintenance of adipose tissue–resident regulatory T cells. *Nat. Immunol.* **16**, 276–285 (2015).

46. Du, N. et al. EGR2 is critical for peripheral naïve T-cell differentiation and the T-cell response to influenza. *Proc. Natl. Acad. Sci. USA* **111**, 16484–16489 (2014).

47. Backer, R.A. et al. A central role for Notch in effector CD8 + T cell differentiation. *Nat. Immunol.* **15**, 1143–1151 (2014).

48. Nakanishi, Y., Lu, B., Gerard, C. & Iwasaki, A. CD8 + T lymphocyte mobilization to virus-infected tissue requires CD4 + T-cell help. *Nature* **462**, 510–513 (2009).

49. Bos, R. & Sherman, L.A. CD4 + T-cell help in the tumor milieu is required for recruitment and cytolytic function of CD8 + T lymphocytes. *Cancer Res.* **70**, 8368–8377 (2010).

50. Yamazaki, C. et al. Critical roles of a dendritic cell subset expressing a chemokine receptor, XCR1. *J. Immunol.* **190**, 6071–6082 (2013).

51. Fossum, E. et al. Vaccine molecules targeting Xcr1 on cross-presenting DCs induce protective CD8 + T-cell responses against influenza virus. *Eur. J. Immunol.* **45**, 624–635 (2015).

52. Yi, J.S., Cox, M.A. & Zajac, A.J. T-cell exhaustion: characteristics, causes and conversion. *Immunology* **129**, 474–481 (2010).

53. Baitsch, L. et al. Exhaustion of tumour-specific CD8 + T cells in metastases from melanoma patients. *J. Clin. Invest.* **121**, 2350–2360 (2011).

54. Steinert, E.M. et al. Quantifying memory CD8 T cells reveals regionalization of immunosurveillance. *Cell* **161**, 737–749 (2015).

55. Schön, M.P. et al. Mucosal T lymphocyte numbers are selectively reduced in integrin alpha E (CD103)-deficient mice. *J. Immunol.* **162**, 6641–6649 (1999).

56. Zhang, N. & Bevan, M. Transforming growth factor-β signaling controls the formation and maintenance of gut-resident memory T cells by regulating migration and retention. *Immunity* **39**, 687–696 (2013).

57. McMaster, S.R., Wilson, J.J., Wang, H. & Kohlmeier, J.E. Airway-resident memory CD8 T cells provide antigen-specific protection against respiratory virus challenge through rapid IFN-γ production. *J. Immunol.* **195**, 203–209 (2015).

58. Clark, R.A. Resident memory T cells in human health and disease. *Sci. Transl. Med.* **7**, 269rv1 (2015).

59. Schenkel, J.M., Fraser, K.A., Vezys, V. & Masopust, D. Sensing and alarm function of resident memory CD8 + T cells. *Nat. Immunol.* **14**, 509–513 (2013).

60. Crawford, A. et al. Immunity resource molecular and transcriptional basis of CD4 + T cell dysfunction during chronic infection. *Immunity* **40**, 289–302 (2014).

61. Day, C., Patel, R., Guillen, C. & Wardlaw, A.J. The chemokine CXCL16 is highly and constitutively expressed by human bronchial epithelial cells. *Exp. Lung Res.* **35**, 272–283 (2009).

62. Geissmann, F. et al. Intravascular immune surveillance by CXCR6 + NKT cells patrolling liver sinusoids. *PLoS Biol.* **3**, 0650–0661 (2005).

63. Hudspeth, K. et al. Human liver-resident CD56bright/CD16neg NK cells are retained within hepatic sinusoids via the engagement of CCR5 and CXCR6 pathways. *J. Autoimmun.* **66**, 40–50 (2016).

64. Lugthart, G. et al. Human lymphoid tissues harbor a distinct CD69 + CXCR6 + NK cell population. *J. Immunol.* **197**, 78–84 (2016).

65. Mohan, K. & Issekutz, T.B. Blockade of chemokine receptor CXCR3 inhibits T cell recruitment to inflamed joints and decreases the severity of adjuvant arthritis. *J. Immunol.* **179**, 8463–8469 (2007).

66. Sporici, R. & Issekutz, T.B. CXCR3 blockade inhibits T-cell migration into the CNS during EAE and prevents development of adoptively transferred, but not actively induced, disease. *Eur. J. Immunol.* **40**, 2751–2761 (2010).

67. Wu, X., Lahiri, A., Haines, G.K., Flavell, R.A. & Abraham, C. NOD2 regulates CXCR3-dependent CD8 + T cell accumulation in intestinal tissues with acute injury. *J. Immunol.* **192**, 3409–3418 (2014).

68. Al-Banna, N.A., Vaci, M., Slauenwhite, D., Johnston, B. & Issekutz, T.B. CCR4 and CXCR3 play different roles in the migration of T cells to inflammation in skin, arthritic joints, and lymph nodes. *Eur. J. Immunol.* **44**, 1633–1643 (2014).

69. Mikucki, M.E. et al. Non-redundant requirement for CXCR3 signalling during tumoricidal T-cell trafficking across tumour vascular checkpoints. *Nat. Commun.* **6**, 7458 (2015).

70. Ray, S.J. et al. The Collagen Binding < α1β1 integrin VLA-1 regulates CD8 T cell-mediated immune protection against heterologous influenza infection. *Immunity* **20**, 167–179 (2004).

71. Cheuk, S., Schlums, H., Bryceson, Y.T., Eidsmo, L. & Tjernlund, A. CD49a expression defines tissue-resident CD8 + T cells poised for cytotoxic function in human skin. *Immunity* **46**, 287–300 (2017).

72. Piet, B. et al. CD8 + T cells with an intraepithelial phenotype upregulate cytotoxic function upon influenza infection in human lung. *J. Clin. Invest.* **121**, 2254–2263 (2011).

73. Takamura, S. et al. Specific niches for lung-resident memory CD8 + T cells at the site of tissue regeneration enable CD69-independent maintenance. *J. Exp. Med.* **213**, 3057–3073 (2016).

74. Iijima, N. & Iwasaki, A. A local macrophage chemokine network sustains protective tissue-resident memory CD4 T cells. *Science (80-.)* **346**, 93–98 (2014).

75. Bergsbaken, T. & Bevan, M.J. Proinflammatory microenvironments within the intestine regulate the differentiation of tissue-resident CD8 + T cells responding to infection. *Nat. Immunol.* **16**, 406–414 (2015).

76. Ganesan, A.-P. et al. Tissue-resident memory features are linked to the magnitude of cytotoxic T cell responses in human lung cancer. *Nat. Immunol.* **18**, 940–950 (2017).

77. Nakano, H. et al. Pulmonary CD103 + dendritic cells prime Th2 responses to inhaled allergens. *Mucosal Immunol.* **5**, 53–65 (2011).

78. Ali, M., Heyob, K. & Rogers, L.K. DHA suppresses primary macrophage inflammatory responses via Notch 1/ Jagged 1 signaling. *Nat. Publ. Gr.* **6**, 22276 (2016).

79. Amsen, D., Helbig, C. & Backer, R.A. Notch in T cell differentiation: all things considered. *Trends Immunol.* **36**, 802–814 (2015).

80. Bailis, W. et al. Notch simultaneously orchestrates multiple helper T cell programs independently of cytokine signals. *Immunity* **39**, 148–159 (2013).

81. Vieira Braga, F.A. et al. Blimp-1 homolog Hobit identifies effector-type lymphocytes in humans. *Eur. J. Immunol.* **45**, 2945–2958 (2015).

82. van Gisbergen, K. P. J. M. et al. Mouse Hobit is a homolog of the transcriptional repressor Blimp-1 that regulates NKT cell effector differentiation. *Nat. Immunol.* **13**, 864–86871 (2012).

83. Holt, P.G. et al. Extraction of immune and inflammatory cells from human lung parenchyma: evaluation of an enzymatic digestion procedure. *Clin. Exp. Immunol.* **66**, 188–200 (1986).

84. Shi, W., Oshlack, A. & Smyth, G.K. Optimizing the noise versus bias trade-off for Illumina whole genome expression BeadChips. *Nucleic Acids Res.* **38**, e204 (2010).